T. Meissner, F. Wentz, D. LeVine, P. De Mattheis

Addendum IV to ATBD

T. Meissner, F. Wentz, D. Le Vine and P. de Matthaeis

July 15, 2015

This addendum documents the changes made to the ATBD between release of V3.0 and V4.0 of the Aquarius L2 salinity retrieval algorithm and included in V4.0. Prior to release of V4.0 the code was updated to include all the changes described here and then the entire data set was rerun.

In brief, the algorithm changes are:

1. The hybrid antenna patterns were used to re-deriving the correction tables for solar intrusion and intrusion from land. They were also used for deriving new values for the antenna gain weighted land fraction g_{land} and the gain weighted sea ice fraction g_{ice}. The galactic correction tables are unchanged from V3.0. The APC coefficients themselves are also unchanged from V3.0.

2. The bias adjusted SSS option available in V3.0 has been removed and is included V4.0 as part of the basic retrieval. This was done by making a small adjustment to the SST dependence of the surface emissivity model that mitigates the observed SST dependent biases. The adjustment is done at the TB level in the geophysical model function and depends on the horn and polarization.

3. An empirical correction has been included to account for the observed non-linear coupling of the 3rd Stokes parameter U into the 1st Stokes parameter I. The reason for this residual (i.e. not corrected by the APC) is unknown.

4. Each salinity retrieval is accompanied by an estimate of its random and systematic uncertainty. The method for computing this uncertainty is described in a separate addendum to the ATBD [Meissner, 2015].

5. Parameters in RFI filter algorithm have been updated to reflect differences in the algorithm for land and ocean. New values of the σ_S parameter that specifies the NEDT in the RFI filtering have been added over land scenes. This parameter is unchanged over ocean scenes.

6. Density is included in V4.0 as a new data product.

7. A correction for significant wave height that was accidently left out of V3.0 is now included in V4.0. The description of this correction was included in Addendum III and is not repeated here.

1 Construction and Use of Hybrid Antenna Patterns

The Aquarius Cold Sky Calibrations demonstrated that neither model available for the Aquarius antenna patterns (i.e. GRASP model or measurements using the scale model measurements) were a good fit and a hybrid pattern was developed [Dinnat et al, 2015]. One consequence of the poor fit was calibration errors at the cold (cold sky) and warm (land) extremes. In V3.0 an empirical adjustment was made to the APC (e.g. to the A-matrix) that improved this calibration problem but a corresponding adjustment to parameters that are computed from the antenna pattern (e.g. the gain weighted fraction gland) were not made. This has been corrected in V4.0.

For V4.0, hybrid antenna patterns have been constructed for all 6 Aquarius channels. The goal is to create antenna patterns that are consistent with the empirically adjusted APC (antenna pattern correction) employed in V3.0. The hybrid antenna patterns have the same cross-polarization values as in the GRASP June 2012 model patterns but the spillover of the pre-launch scale model patterns (which is about 1 – 1.5% smaller than the GRASP 2012 spillover values).
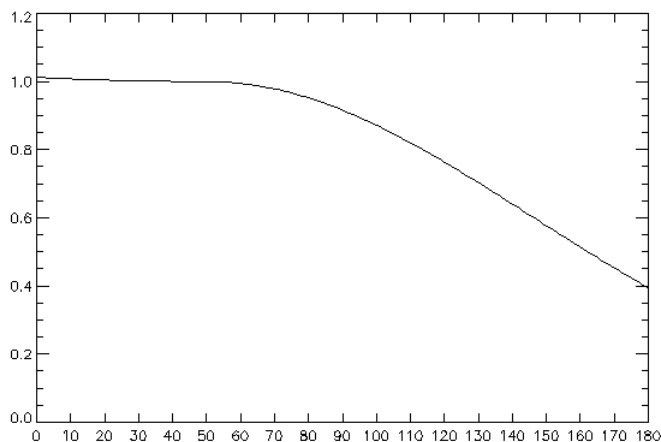
Figure 1: Scaling of the antenna gain as function of the polar angle θ (x-axis, in deg) that is used in the construction of the hybrid antenna patterns.

In order to construct these patterns a scaling procedure has been developed that transfers power from the antenna backlobes into the main lobe and near-sidelobes (Figure 1). The scaling depends on the polar angle θ (zero at antenna boresight). The value for the transition angle where the value of the scaling function is 1.0 was set to $\theta_c=50^\circ$, which is consistent with a similar analysis that was performed by [Dinnat et al, 2015].

The form of our scaling function is:

$$s(\theta) = \begin{cases} \exp\left[+\alpha \cdot (\theta - \theta_c)^2\right], & \theta \le \theta_c \\ \exp\left[-\beta \cdot (\theta - \theta_c)^2\right], & \theta > \theta_c \end{cases} \qquad (1)$$

The value of the polar angle θ is in degrees. The values for the constants α and β for each channel are listed in Table 1.

Table 1: Values for the constants α and β in the AP scaling (1) for each Aquarius channel.

Channel	α	β
1V	0.500E-5	5.500E-5
1H	0.800E-5	8.200E-5
2V	0.480E-5	6.000E-5
2H	0.820E-5	11.500E-5
3V	0.430E-5	6.300E-5
3H	0.670E-5	9.300E-5

Table 2: Coefficients of the matrix used in the antenna pattern correction (APC). Shown are the A-matrix elements derived using the GRASP 2012 pattern (left), the A-matrix in V3.0 (center) and the A-matrix using the hybrid patterns (right). The A-matrices are written in Stokes components (I, Q, U). The first row is I.

horn 1
```
1    1.04484  -0.03827  -0.00387
2   -0.00297   1.07860   0.03089
3   -0.00009  -0.02582   1.07551
```

horn 1
```
1    1.0300   -0.0350   +0.0500
2    0.0001    1.0641   +0.0300
3    0.0000   -0.0258    1.0755
```

horn 1
```
1    1.0300   -0.0350   +0.0500
2    0.0001    1.0641   +0.0300
3    0.0000   -0.0258    1.0755
```

horn 2
```
1    1.04967  -0.03432  -0.00737
2   -0.00063   1.05936  -0.01558
3   -0.00272   0.01112   1.05553
```

horn 2
```
1    1.0337   -0.0304    0.0000
2    0.0027    1.0435   -0.0144
3   -0.0006   +0.0211    1.0555
```

horn 2
```
1    1.0337   -0.0304    0.0000
2    0.0027    1.0435   -0.0144
3   -0.0006   +0.0211    1.0555
```

horn 3
```
1    1.05800  -0.03435  -0.01157
2   -0.00036   1.04848   0.00708
3   -0.00324  -0.01480   1.04885
```

horn 3
```
1    1.0420   -0.0326   +0.0250
2    0.0011    1.0328   +0.0215
3    0.0000   -0.0148    1.0489
```

horn 3
```
1    1.0420   -0.0326   +0.0250
2    0.0011    1.0328   +0.0215
3    0.0000   -0.0148    1.0489
```

Table 3: Values for the spillover value η for the GRASP 2012 patterns, the APC in V3.0 and the hybrid patterns.

Channel	GRASP 2012	V3.0	Hybrid
1V	0.04018	0.02923	0.02948
1H	0.04545	0.02902	0.02896
2V	0.04669	0.03516	0.03611
2H	0.04788	0.03016	0.03096
3V	0.05447	0.04134	0.04463
3H	0.05508	0.03934	0.04164

The elements of the A-matrix for the hybrid patterns are listed in Table 2, which also compares with the value from GRASP 2012 and the A-matrix used in V3.0. The corresponding

3

spillover values are listed in Table 3. The definitions used are the same as in [Meissner, 2013]. The APC employed in V4.0 uses the same A-matrix as V3.0. The spillover values that are produced by the hybrid patterns are very close, though not exactly the same as the ones that were used in V3.0. In the V4.0 processing the hybrid antenna patterns are used for deriving the antenna gain weighted fractions for land g_{land} and sea ice g_{ice} as well as the correction tables for land intrusion and the direct and reflected solar intrusions. This improves the consistency between these parameters and the APC matrix.

The corrections for the direct and reflected galactic radiation have not been changed in V4.0. It is planned to do that for a future release. The reason for waiting is that a small but noticeable error has been detected in the processing of the galactic maps itself upon which the derivation of the correction tables is based. As a consequence, the whole galactic correction including the zonal symmetrization procedure (Addendum III) will need to be revisited. We have also not changed the correction for the backscattered solar radiation, as its size is very small.
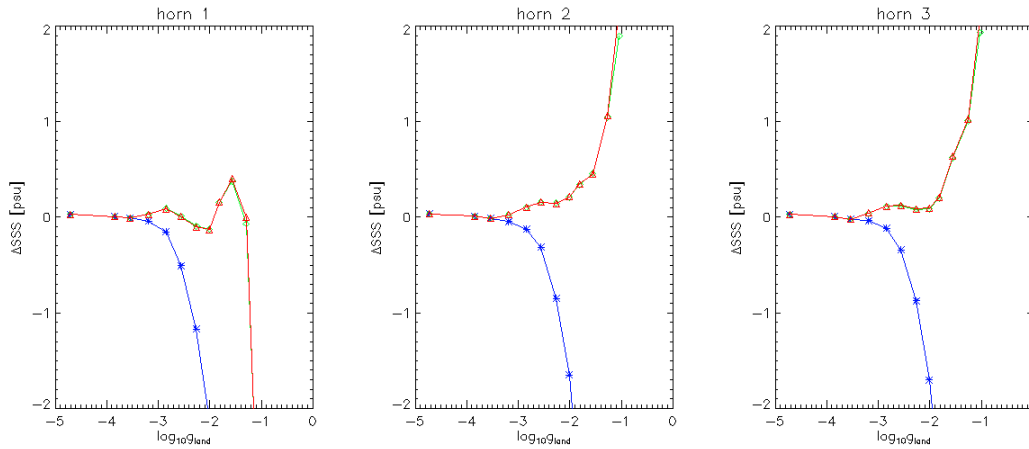
Figure 2: Bias between Aquarius and HYCOM SSS as function of gain weighted land fraction g_{land} (logarithmic x-axis). Blue curve: no land correction. Green curve: Land correction of V3.0. Red curve: Land correction of V4.0.
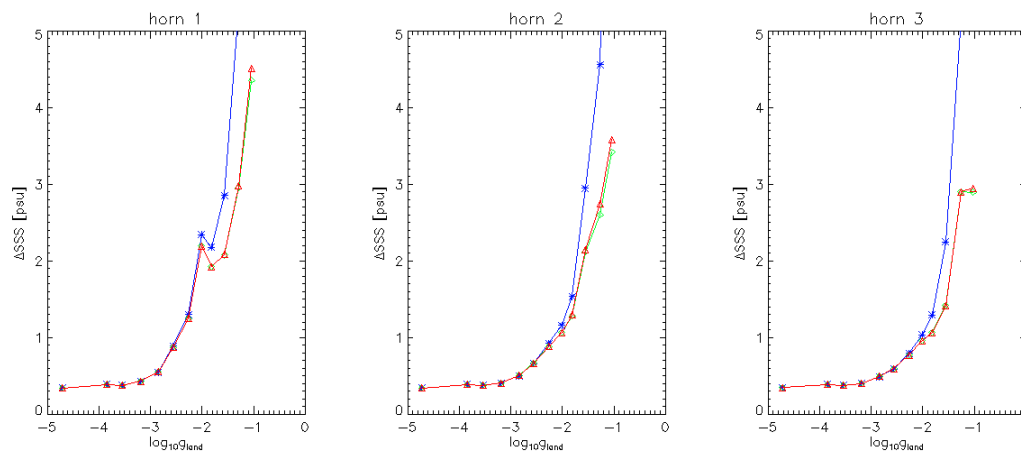
Figure 3: Same as Figure 2 for the standard deviation between Aquarius and HYCOM SSS.

The effect of using the hybrid patterns in V4.0 on the salinity retrievals compared with the V3.0 is extremely small and has negligible impact. The introduction of the hybrid antenna patterns in V4.0 was done for consistency reasons rather than its actual impact on the retrieved SSS. The impact of the new antenna patterns can be seen by examining the degradation of the Aquarius SSS as a function of contamination from land. This can be seen by comparing the difference between Aquarius and HYCOM SSS as function of gland (Figure 2 and Figure 3). No noticeable change from V3.0 (green curves) to V4.0 (red curves) occurs. These two figures also demonstrate the improvement to the SSS retrievals by including the land correction compared with doing no land correction at all (blue curves) which is the same as before.

2   Empirical Adjustment of Surface Emissivity

2.1   Analysis of Large Scale Biases in the Aquarius V3.0 Standard Salinities

When compared to ARGO measurements or the HYCOM model, the standard ADPS Version 3.0 salinity product exhibits fresh biases in the tropics and salty biases at high northern and southern latitudes. These biases correlate clearly with SST. For V3.0 a simple post-hoc SST dependent adjustment to the salinity was derived and included as additional product in the ADPS V3.0 data release (Addendum III). It is suspected that the bias arises due to inaccuracies in the geophysical model function used in the salinity retrieval algorithm, although a more thorough investigation as to the physical cause of the SST dependent biases is in order.

2.2   Analysis of Possible Physical Causes
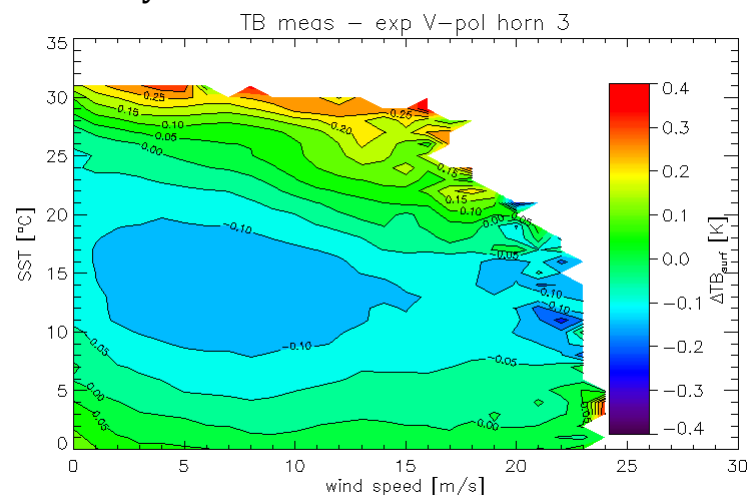
Figure 4: Difference between measured and expected surface TB of Aquarius horn 3 V-pol in V.3.0 as function of SST and wind speed. For the computation of the expected TB the HYCOM salinity field was used.

As a first step in the search for causes, an analysis has been performed of the residual difference in measured minus expected TB for all 6 Aquarius channels as function of both SST and wind speed. All events have been filtered for rain using rain retrievals from either the CONAE K/Ku-band microwave radiometer MWR or one of the microwave imagers (SSMIS F17,

WindSat, TMI) that were collocated to Aquarius within 1 hour. Figure 4 shows the result for horn 3 v-pol. The results for the other five Aquarius channels look very similar. A close look at Figure 4 suggests that at least two different mechanisms are responsible.

At SST above 25℃, which correlates with the observed fresh biases in low latitudes, the difference between measured and computed TB clearly increases with wind speed and becomes small at low winds. That indicates that the bias could be caused by the SST (T_S) dependence assumed in the wind induced emissivity model ΔE_W (W, T_S) that is used in the surface roughness correction [Meissner et al., 2014]. The roughness model that is used in the V3.0 retrieval algorithm assumes that ΔE_W is proportional to the specular E_0 (T_S), which is based on the geometric optics model. We know that other mechanisms beyond the assumptions of the geometric optics model are important for the surface roughness at L-band frequencies, for example Bragg scattering and at higher wind speeds and also sea foam. Those mechanisms have a different SST dependence and it is therefore conceivable that the assumed SST dependence in the surface roughness model needs to be adjusted.
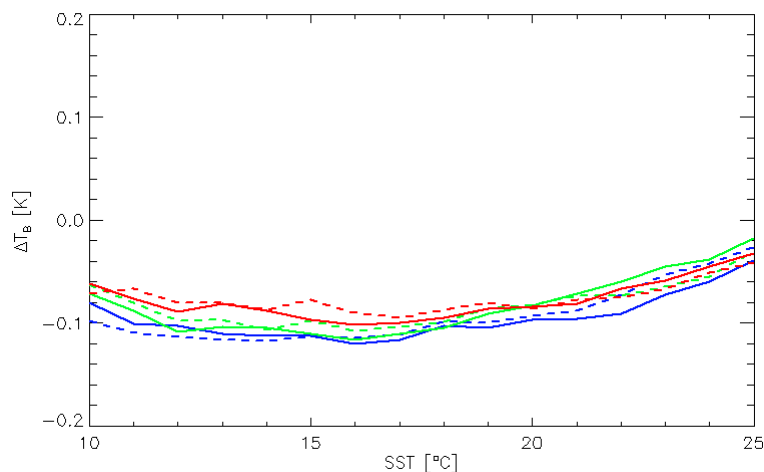
Figure 5: Observed biases in TB measured – computed: blue = horn 1, green = horn 2, red = horn 3, full lines = v-pol, dashed lines = h-pol.

At SST below 25℃ the biases appear to show little correlation with wind speed and are therefore unlikely related to the wind induced emissivity model. The most likely causes for these biases are:

1. The dielectric model of sea water describing the microwave emission from flat ocean surfaces at L-band frequencies [Meissner and Wentz, 2004, 2012].

2. The model for oxygen absorption that is used in the retrieval algorithm to correct for atmospheric attenuation. The oxygen absorption depends on atmospheric temperature, which strongly correlates with SST. AT L-band the oxygen absorption comes from the non-resonant continuum, where accurate measurements are difficult and rare. The non-resonant oxygen continuum absorption model that is used in the V3.0 algorithm is based on the work of Liebe [1985, 1989], which itself cites an old work by Minglegrin [1974]. An empirical adjustment to the temperature dependence of this continuum absorption

that was based on WindSat and AMSR TB observations at C-band and X-band has already been made in the oxygen absorption model that was used in V3.0 and all prior versions of the algorithm.

A study has been performed showing that small uncertainties well within the margins of errors of these models can easily cause the observed SST dependent biases for SST below 25^{0}C. This is demonstrated in Figure 5, Figure 6 and Figure 7. Other possible causes of the observed biases are biases in the ancillary SST field itself or differences between the air and the sea surface temperature. A more detailed analysis of those effects is planned for the future.
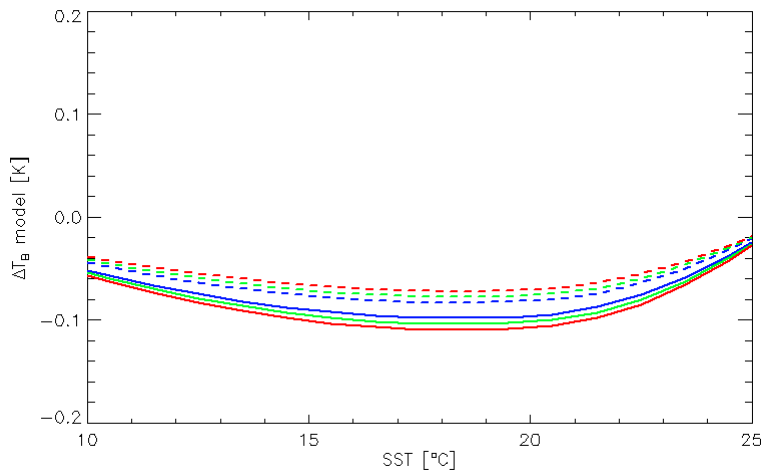
Figure 6: Biases in TB that are created by a 0.3% error in the imaginary part of the dielectric constant of sea water. The labelling of the curves is the same as in Figure 5.
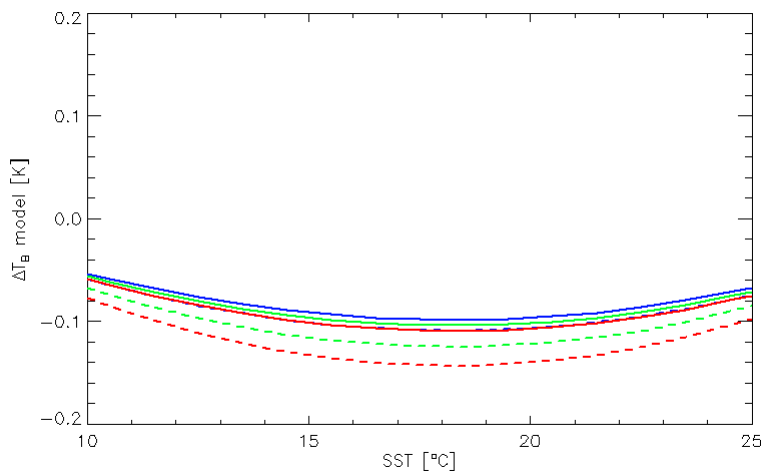
Figure 7: Biases in TB created by a 2% error in the atmospheric oxygen absorption model. The labelling of the curves is the same as in Figure 5.

2.3   Form of the Empirical Model Function Adjustment

The magnitude of the GMF update that accounts for the observed biases is very small (0.1 – 0.2 K) and lies within the uncertainties of the geophysical models that are used. As an example of a typical model error one can consider the difference between surface emitted brightness temperature that are computed by the   Meissner-Wentz [Meissner and Wentz, 2004] and the Klein-Swift [Klein and Swift, 1977] dielectric models exceeds this value. It is difficult to unequivocally disentangle all the potential physical causes listed in section 2.2 and to change the parameters in the models accordingly. Also these model functions (e.g. for the dielectric constant of seawater and the oxygen absorption model) are functions of frequency and any changes at L-band potentially will require adjustments at higher frequencies. Therefore it was decided to perform a small empirical adjustment of the surface emissivity model for each of the six channels, which effectively accounts for the observed biases. The form of the TB adjustment $\Delta T_{B,1}$ as function of surface temperature T_S and Aquarius HHH wind speed W is:

$$\Delta T_{B,1}(T_S,W) = T_S \cdot \Delta E_1(T_S,W)$$
$$\Delta E_1(T_S,W) = \delta(T_S), \qquad\qquad \text{if}\quad T_S \leq T_t \qquad\qquad (2)$$
$$\Delta E_1(T_S,W) = \delta(T_S) \cdot \frac{A_0(W)}{A_0(W_t)}, \quad \text{if}\quad T_S > T_t$$

In the V4.0 L2 processing the computed value of $\Delta T_{B,1}$ gets added to the surface roughness correction (Addendum III, section 3). That means effectively the value of $\Delta T_{B,1}$ gets subtracted from the measured Aquarius TB before the SSS is retrieved by matching measured and computed TB (Addendum III, section 4). In Equation (2), the function $A_0(W)$ is the 0th harmonic of the wind induced emissivity model function as it was defined in Section 3 and Appendix C of Addendum III. The value of the constant W_t is 7.5 m/s. The values for the transition temperatures T_t depend on channel and lie around 25°C. The SST dependent function δ vanishes at the transition temperature T_t . The numerical values for δ and T_t are tabulated in Table 3**Error! Reference source not found.** and Table 4 of Appendix A.
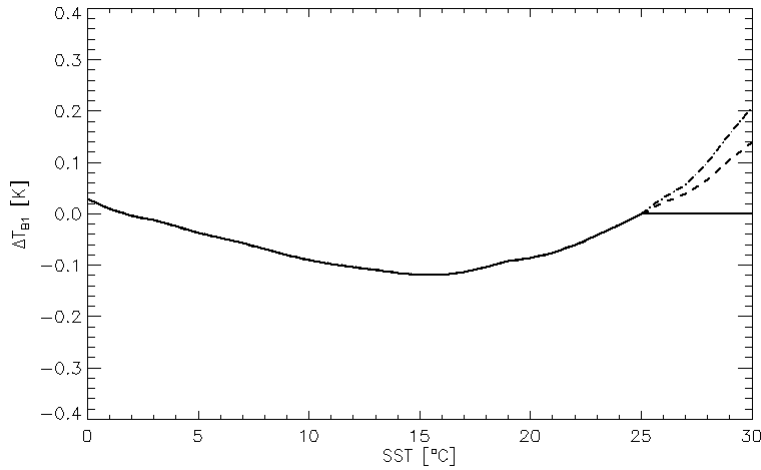
Figure 8: Value of $\Delta T_{B1}(T_S)$ for horn2 H-pol. Full line: W = 0 m/s, dashed line: W = 7.0 m/s, dashed-dot line: W = 12 m/s.

Error! Reference source not found. shows the empirical correction $\Delta T_{B,1}(T_S)$ for horn 2 H-pol for three different wind speeds. The correction is empirical, but the assumption is that below the transition temperature ($T_t = 24.99^{\circ}C$) the correction accounts adjustments required in parameters such as the dielectric constant or oxygen absorption, and above the transition temperature the correction accounts for a small adjustment required on the SST dependence of the wind induced emissivity. The effect on the wind emissivity for horn 3 H-pol is shown in Figure 9.
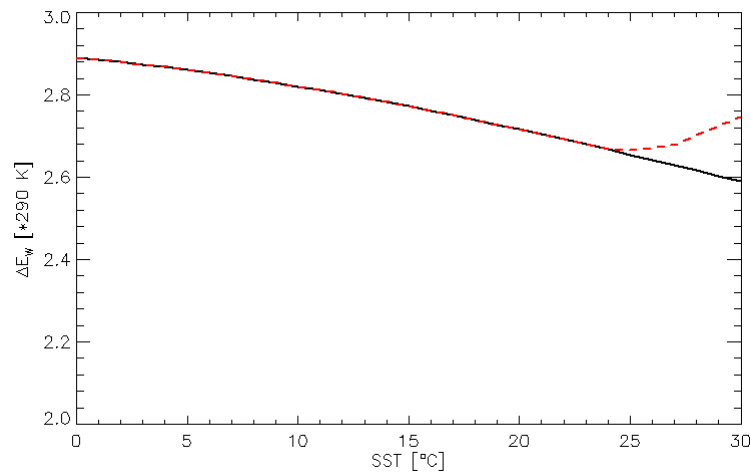
Figure 9: SST dependence of the wind induced emissivity $\Delta E_W(W, T_S)$ for horn 3 H-pol at W = 7.5 m/s. Full black line = V3.0. Dashed red line = V4.0.

3   Non-Linear IU Coupling

All prior data Aquarius data releases, including V3.0, have exhibited a spurious coupling from the 3rd Stokes parameter U into the 1st Stokes parameter I, which results in an error in the retrieved salinity that is correlated with the value of the 3rd Stokes parameter U. These observed biases have also been reported by the University of Hawaii group within an EOF (empirical orthogonal functions) analysis of the spatial and temporal patterns of SSS Aquarius – ARGO.

The full lines in Figure 10 shows the observed biases in TB measured – expected of the I/2 = (V+H)/2 at the TOI as function of the 3rd Stokes TA for the 3 Aquarius horns. For a given value of the 3rd Stokes TA the bias increases with decreasing incidence angle. That means it is smallest for the outer horn and largest for the inner horn.

The bias curves in Figure 10 are non-linear. It is currently not understood what the root cause of the observed bias is and it is also not clear if it is caused by the instrument or some deficiency in the algorithm that transforms the measured antenna temperatures into the TOI TB. If the coupling from 3rd Stokes U_A into the 1st Stokes I was linear, as it is the case for the coupling of U into the 2nd Stokes Q, could be explained by an inaccuracy of the APC coefficients and thus be absorbed into and adjustment of the APC matrix [Meissner, 2014]. This is not the case for a non-linear behavior of the IU coupling as it is shown in Figure 10.
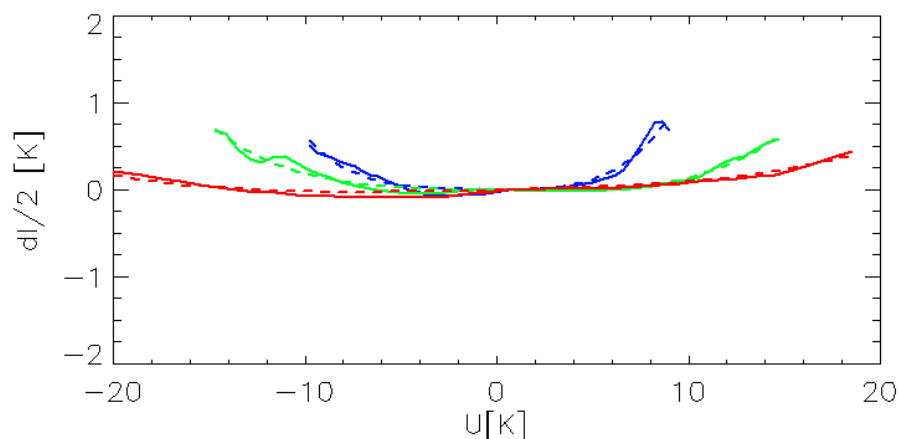
Figure 10: TB measured – expected for I/2 = (V+H)/2 as function of antenna temperature 3rd Stokes U_A for the three Aquarius horns. Blue = horn 1, green = horn 2, red = horn 3. Full lines = observations, dashed lines = 4th polynomial fits.

For the V4.0 processing am empirical correction was implemented in order to account for the observed spurious biases. We have fitted 4th order polynomials (dashed curves in Figure 10) to the observed bias curves (full lines in Figure 10):

$$\frac{\Delta I(U_A)}{2} = \sum_{k=1}^{4} \zeta_k \cdot U_A^k \qquad (3)$$

In the Aquarius V4.0 L2 processing the computed value of $\Delta I(U_A)$ from equation (3) gets subtracted after the APC from the 1st Stokes at the TOI I_{TOI}. The numerical values for the polynomial coefficients ζ_k, k=1,…4 are listed in Table 5Table 5: of Appendix B.

4. RFI Detection/Mitigation Parameters

Version V3.0   Version V4.0
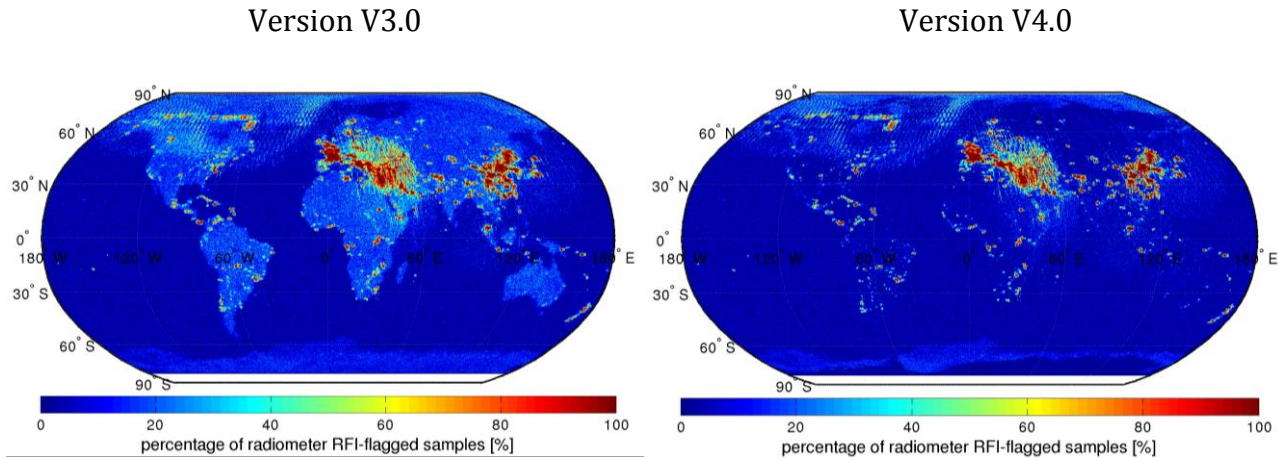
Figure 11: Percentage of radiometer RFI-flagged samples, average of V- and H-polarizations, with V3.0 (left) and V4.0 (right) values of the parameter ta_nom in the RFI flagging algorithm for the period December 1-14, 2011.

The value of the parameter σ_s which determines the thresholds in the RFI filtering (see Section 7 in Aquarius document AQ-014PS-0015 [Piepmeier et al., 2013]) has been made dependent on latitude and longitude. This was done using the grid previously established as an option for the parameters W_m and W_d (but these parameters have been and remain constant everywhere). The grid is the 1-degree UCAR landmask (available at http://www.ncl.ucar.edu/Applications/Data/cdf/landsea.nc). In V4.0 the W_m and W_d remain constant but the parameter, σ_s, takes on different values for land and ocean. For a given 10 ms sample, the RFI algorithm uses the latitude and longitude where the measurement is made and a value of σ_s determined by whether the point is over ocean or land as determined by the UCAR landmask. The values for ocean are:

	beam 1	beam 2	beam 3
V	0.5579	0.5426	0.5517
P	0.5508	0.5621	0.5742
M	0.5398	0.5480	0.5541
H	0.5320	0.5378	0.5456

and over land or sea ice they are:

	beam 1	beam 2	beam 3

11

V	0.7196	0.7069	0.7182
P	0.7311	0.7257	0.7632
M	0.7250	0.7371	0.7401
H	0.6952	0.7088	0.7171

The reason for this code modification is to have the same false alarm rate (approximately 4%) over land and over ocean. This is illustrated in Figure 11, which compares the percentage of detected RFI samples in version V3.0 and V4.0. This change in σ_s has a negligible effect on the soil moisture retrieval with a variation of less than 0.003 m^3/m^3 found.

6. Density

Density is a highly non-linear derived variable which depends on temperature, salinity, and pressure. With the introduction of the Thermodynamic Equation of State in 2010 (TEOS-10), a new thermodynamically consistent formulation of temperature, salinity and density (amongst other variables) was introduced [IOC *et al.*, 2010]. TEOS-10 has been accepted by the Intergovernmental Oceanographic Commission and UNESCO to replace the previously used UNESCO Equation of State 1980 (EOS-80) [UNESCO, 1981]. TEOS-10 introduces a number of new variables that are required for the computation of density from *in-situ* measurements. The two relevant variables for the purposes of computing surface density from Aquarius Sea Surface Salinity (SSS) and the ancillary Sea Surface Temperature (SST) fields are Absolute Salinity (S_A) and Conservative Temperature (Θ).

Thus, to determine surface density from Aquarius-derived and ancillary data fields, S_A and Θ have to be computed prior to calculating the density. It should be noted that while S_A should be used in all scientific publications involving salinity, it is not recommended for archival purposes. For this reason, Aquarius data will continue to be distributed as practical salinity (S_P) as defined by the Practical Salinity Scale (PSS-78) [UNESCO, 1981].

Conservative Temperature (Θ) is similar to potential temperature in EOS-80, but is designed to be conserved both under adiabatic mixing and changes in depth [IOC, 2010], which is fulfilled neither by potential or *in-situ* temperature. Absolute Salinity (S_A) is a true mass fraction, and defined as the mass fraction of the solute in standard seawater with a density that is identical to the sample. Consequently, S_A has units of g kg^{-1}. These definitions are explained in more detail in [IOC, 2010] as well as [Pawlowicz, 2010].

All computations are performed using the Gibbs-Seawater (GSW) Oceanographic Toolbox [McDougall and Barker, 2011] V3.03 for C. In the first step, S_A is computed from S_P using the subroutine *gsw_sa_from_sp*, which requires four inputs, S_P, pressure, longitude and latitude. In the next step, Θ is computed from sea surface temperature [ITS-90, Preston-Thomas, 1990] using the subroutine *gsw_ct_from_t*, which requires S_A, pressure, and temperature as inputs. Having computed all required input variables, density is then determined using the subroutine *gsw_rho*, which requires S_A, Θ, and pressure as input variables. In all these computations, pressure is fixed to a value of 0, as pressure is defined relative to atmospheric pressure.

7. References

Piepmeier, J. et al, AQ-014PS-0015, Aquarius radiometer post-launch calibration for product version 2, www.podaac.jpl.nasa.gov/aquarius, 2013.

Dinnat, E, D. Le Vine, J. Piepmeier, S. Brown and L. Hong, Aquarius L-band radiometers calibration using cold sky, accepted for publication, IEEE JSTARS special issue on Aquarius, 2015.

IOC, SCOR and IAPSO, The international thermodynamic equation of seawater – 2010: Calculation and use of thermodynamic properties, Intergovernmental Oceanographic Commission, Manuals and Guides No. 56, UNESCO (English), www.teos-10.org/pubs/TEOS-10_Manual.pdf, 2010.

Klein, L.A., and C. T. Swift, An improved model for the dielectric constant of sea water at microwave frequencies, IEEE J. Oceanic Eng., vol. OE-2, pp. 104–111, 1977.

Liebe, H. J., An updated model for millimeter wave propagation in moist air, Radio. Sci., vol. 20, pp 1069 – 1089, 1985.

Liebe, H. J., MPM – An atmospheric millimeter-wave propagation model, Int. J. of Infrared Mill. Waves, vol. 10(6), pp 631 – 650, 1989.

McDougall, T.J., and P.M. Barker, Getting started with TEOS-10 and the Gibbs Seawater (GSW) Oceanographic Toolbox, SCOR/IAPSO WG127, ISBN 978-0-646-55621-5, 28pp, www.teos-10.org/pubs/Getting_Started.pdf, 2011.

Meissner, T., and F. Wentz, The complex dielectric constant of pure and sea water from microwave satellite observations, IEEE TGRS, vol. 42, 1836-1849, 2004.

Meissner, T., and F. Wentz, The emissivity of the ocean surface between 6 - 90 GHz over a large range of wind speeds and Earth incidence angles, IEEE TGRS, vol. 50, 3004-3026, 2012.Meissner, T., Memo: Proposed APC Changes from V2.0 to V3.0, 05/19/2013, RSS Tech. Report 05192013, http://podaac.jpl.nasa.gov/SeaSurfaceSalinity/Aquarius, 2013.

Meissner, T., F. Wentz and L. Ricciardulli, The emission and scattering of L-band microwave radiation from rough ocean surfaces and wind speed measurements from the Aquarius sensor, JGR Oceans, vol. 119, doi: 10.1002/2014JC009837, 2014.

Meissner, T., Assessment of Uncertainties in Aquarius Salinity Retrievals, ATBD, RSS Technical Document 061015, 2015, http://podaac.jpl.nasa.gov/SeaSurfaceSalinity/Aquarius. Minglegrin, U., The microwave dispersion spectrum of O_2, Mol. Phys., vol. 28(6), 1591 – 1602, 1974.

Pawlowicz, R., What every oceanographer needs to know about TEOS-10 (The TEOS-10 Primer, Web document, http://www.teos-10.org/pubs/TEOS-10_Primer.pdf, 2010.

Preston-Thomas, H., 1990: The International Temperature Scale of 1990 (ITS-90). Metrologia, 27(1), pp 3-10, http://www.omega.com/temperature/z/pdf/z186-193.pdf, 1990.

UNESCO, 1981: The Practical Salinity Scale 1978 and the International Equation of State of Seawater 1980. UNESCO technical papers in marine science 36, http://www.jodc.go.jp/info/ioc_doc/UNESCO_tech/046148eb.pdf, 1981.

Appendix A.
Tabulated Values for T_t and δ of the Empirical Emissivity Adjustment in Section 2.3

Table 3: Values of the function $\delta\left(T_S\right)$ [in Kelvin] from equation (2).

TS	1V	1H	2V	2H	3V	3H
-2.0	0.181	0.152	0.131	0.101	0.074	0.032
-1.0	0.15	0.123	0.098	0.082	0.053	0.018
0.0	0.12	0.095	0.066	0.064	0.032	0.003
1.0	0.087	0.066	0.032	0.045	0.009	-0.012
2.0	0.066	0.04	0.007	0.03	-0.005	-0.021
3.0	0.048	0.018	-0.011	0.017	-0.012	-0.029
4.0	0.026	0.002	-0.032	-0.002	-0.025	-0.041
5.0	0.009	-0.016	-0.053	-0.015	-0.039	-0.048
6.0	-0.006	-0.029	-0.065	-0.024	-0.049	-0.06
7.0	-0.021	-0.041	-0.073	-0.041	-0.058	-0.072
8.0	-0.039	-0.061	-0.088	-0.056	-0.07	-0.077
9.0	-0.058	-0.076	-0.105	-0.068	-0.083	-0.086
10.0	-0.071	-0.091	-0.121	-0.081	-0.092	-0.098
11.0	-0.082	-0.105	-0.134	-0.092	-0.099	-0.11
12.0	-0.092	-0.112	-0.137	-0.1	-0.106	-0.114
13.0	-0.1	-0.114	-0.145	-0.105	-0.111	-0.12
14.0	-0.107	-0.119	-0.149	-0.11	-0.116	-0.129
15.0	-0.112	-0.124	-0.146	-0.114	-0.12	-0.13
16.0	-0.112	-0.121	-0.143	-0.113	-0.118	-0.13
17.0	-0.105	-0.114	-0.134	-0.103	-0.114	-0.127
18.0	-0.096	-0.1	-0.122	-0.092	-0.102	-0.117
19.0	-0.089	-0.088	-0.107	-0.085	-0.092	-0.103
20.0	-0.079	-0.08	-0.092	-0.076	-0.085	-0.093
21.0	-0.071	-0.071	-0.075	-0.065	-0.075	-0.082
22.0	-0.059	-0.054	-0.059	-0.053	-0.059	-0.066
23.0	-0.039	-0.031	-0.034	-0.033	-0.039	-0.047
24.0	-0.015	-0.012	-0.008	-0.008	-0.022	-0.03
25.0	0.009	0.013	0.02	0.015	0	-0.006
26.0	0.022	0.036	0.042	0.03	0.021	0.016

27.0	0.034	0.05	0.055	0.049	0.038	0.036
28.0	0.064	0.078	0.082	0.081	0.067	0.065
29.0	0.118	0.125	0.13	0.129	0.105	0.107
30.0	0.181	0.176	0.19	0.186	0.14	0.159
31.0	0.242	0.226	0.247	0.242	0.176	0.209
32.0	0.303	0.276	0.304	0.296	0.211	0.258

Table 4: Numerical values for the transition temperature T_t in equation (2).

Channel	1V	1H	2V	2H	3V	3H
Value of T_t [ºC]	24.60	24.29	24.51	24.99	24.34	25.22

Appendix B.
Values for the Coefficients ζ_k of the Non-Linear IU Coupling in Section 3

Table 5: Numerical Values for the Coefficients $\zeta_k, k = 1, \ldots 4$ in equation (3) for the three Aquarius horns.

k	1	2	3	4
horn 1	-1.58755100e-003	1.71341502e-003	3.18569692e-004	7.46477289e-005
horn 2	-2.35805891e-003	4.11458555e-004	-1.00910563e-006	1.22936368e-005
horn 3	5.25833641e-003	2.56355465e-004	6.95031563e-006	1.47258597e-006